Prioritization of PMU Location and Signal Selection for Monitoring Critical Power System Oscillations

Tong Huang ⓘ, *Student Member, IEEE*, Meng Wu, *Student Member, IEEE*, and Le Xie ⓘ, *Senior Member, IEEE*

Abstract—This paper proposes a method of selecting and/or locating phasor measurement unit (PMU) signals for monitoring critical oscillation modes in large power systems. A robust indicator, modal participation ratio, is introduced to identify critical PMU locations and signal channels, in order to monitor modes of interest to power system operators. This indicator is easy to compute in practice, and is theoretically rigorous based on linear control theory and spectral analysis. This indicator can suggest location and/or selection of PMUs in order to most effectively observe modes of interest to power system operators. The effectiveness and robustness of the algorithm is illustrated in both modified 68-bus system and 140-bus system.

Index Terms—Oscillation monitoring, phasor measurement unit (PMU), modal participation ratio (MPR).

I. INTRODUCTION

PHASOR measurement units (PMU) offer time-stamped measurements with high sampling rate and consequently are considered as a significant role for improving wide-area monitoring, protection and control (WAMPAC) in the future grid [1]. One key advantage of PMU systems compared with the traditional supervisory control and data acquisition (SCADA) systems is that, PMU systems can be applied to real-time monitoring of electromechanical oscillations, thanks to the high sampling rates of PMUs. Comparing with damped oscillations, sustained oscillations draw more attention of system operators, since it indicates stability issues of the system, therefore corrective actions need be taken once they are observed. However, due to the uneven distribution of modal information among various measurements [2], [3], some oscillation modes could only be monitored clearly through several critical PMU devices and signal channels, thereby causing the different significance of signals in terms of monitoring critical oscillations. As the coverage rate of PMUs increases in recent years, although all PMU signals feeding to control centers are supposed to be utilized in a proper manner, the signals rich of critical modal information should be processed with top priority in the context of

oscillation monitoring, given the high cost of computation and communication. Therefore, one natural question from the perspective of system operators is that, which PMU device(s) and signal channel(s) could provide the sufficient observability for critical oscillations of their interest, and whether further PMU deployments are necessary for monitoring critical oscillations. In other words, PMUs should be selected and/or placed in such a way that all modes of interest should manifest themselves as dominant modes, instead of being hidden, in the signals selected for observing them, once these modes are excited.

In view of the above question raised by system operators, several approaches can be applied to identify critical PMU locations for oscillation monitoring. The basic idea of these approaches is to design an indicator to quantify the coupling between modes and measurements, then the locations of PMUs for observing critical modes are ranked based on the indicator. The indicator can be calculated using both data-driven and model-based approach. The initial purpose of data-driven approaches is to select signals for power system ambient modal estimation (AME) introduced in [4], [5]. In [6], two factors to quantify the steepness and distinctness of the spectrum of the modes are defined to select signals for AME. However, these factors are calculated based on the measurements of existing PMUs. Hence, no suggestion on the further deployment of PMUs is offered, if some modes of interest cannot be observed using existing PMUs. In [7], based on the parametric models identified from measured or simulated data, the variance of estimated damping ratios serves as an indicator to rank the signals for estimating critical modes. This approach is based on an identified statistic model. However, not all critical modes can be reliably included in the identified model, and the modes estimated from the identified model might contain numerical artifacts [3], lacking of valid physical explanations, due to the issue of model-structure selection. In fact, abundant modal information can be computed from the first-principle model of power system. Thus, a fundamental question is how to describe the coupling between oscillation modes and measurements via the first-principle model directly, instead of going through the procedure of system identification, if a well-formed system model is available.

In order to answer the preceding question, two existing indicators based on system models seem to be able to suggest location and/or selection of PMUs. A participation factor (PF) initially introduced in [8] is applied to studying the coupling between oscillation modes and system state variables. However, the PF cannot provide the coupling between oscillation modes and system outputs (i.e., PMU measurements), rendering it ineffective

for addressing the above problem. In [9], a geometric measure (GM) is proposed for quantifying the observability of a particular oscillation mode in system outputs. The GM is further applied to PMU placement problems for maximizing observability of modes of interest [10] and selecting control loop for wide-area controllers (WAC) [11]. However, one insight from [7], [12], [13] is that the distribution of modal parameter over the measurements depends both on the inherent property of the system model and the characteristic of excitation in most practical cases,[1] whereas the GM is calculated from linearized system model without taking any information from disturbance. Besides, the physical meaning of quantified modal observability is still an open question. For example, does a signal with high observability indicate the mode is dominant in the given signal in terms of the spectral analysis? Thus, an theoretically rigorous indicator containing information from both the system and the disturbance is need to be designed for prioritization or placement of PMUs.

In this paper, a robust indicator, modal participation ratio (MPR), is introduced for identifying critical PMU locations and signal channels, in order to better monitor power system oscillations with specific oscillation modes. By exploiting both the off-line model and the characteristic of disturbance in power system, the indicator is calculated and applied for prioritizing the PMUs in terms of observing critical modes. An algorithm embedded with the proposed MPR is presented for the following purposes: 1) it systematically identifies existing PMU devices and signal channels, which provides the best observability for critical oscillation modes; 2) it suggests the optimal locations for further PMU deployments, in order to enhance the observability for critical oscillation modes.

The rest of the paper is organized as follows. Section II provides analytical decomposition of the PMU measurements into various modes; Section III presents newly-introduced factor MPR and the two-layer algorithm; Section IV validates the performance of the proposed algorithm via simulation studies; Section V summarizes this paper.

II. DECOMPOSITION OF PMU MEASUREMENTS INTO VARIOUS MODES

The power system small-signal dynamics around a certain operating condition can be described using the following linearized differential and algebraic equations (DAEs):

$$\dot{\boldsymbol{x}} = A\boldsymbol{x} + B\boldsymbol{u} \tag{1a}$$

$$\boldsymbol{y} = C\boldsymbol{x} \tag{1b}$$

where $\boldsymbol{x} \in \mathbb{R}^n$ is the internal state vector, representing the state deviation from the steady state of the system; $\boldsymbol{y} \in \mathbb{R}^m$ and $\boldsymbol{u} \in \mathbb{R}^d$ include m potential measurements and d inputs, respectively. $n \times n$ matrix A results from the linearizion of corresponding non-linear system around the equilibrium point. Let $(\lambda_1, \lambda_2, \ldots, \lambda_n)$, $(\boldsymbol{r}_1, \boldsymbol{r}_2, \ldots, \boldsymbol{r}_i, \ldots, \boldsymbol{r}_n)$ and $(\boldsymbol{l}_1^T, \boldsymbol{l}_2^T, \ldots, \boldsymbol{l}_i^T, \ldots, \boldsymbol{l}_n^T)^T$ denote matrix A's n distinct eigenvalues, n right eigenvectors and n left eigenvectors, respectively,

[1]The cases exclude the modes that are either unobservable or uncontrollable.

where column vector $\boldsymbol{r}_i \in \mathbb{C}^n$ and row vector $\boldsymbol{l}_i \in \mathbb{C}^n$ are right and left eigenvectors associating with λ_i, respectively. Each state variable is typically coupled with others in the state vector $\boldsymbol{x}$ because of the non-diagonal matrix A. Then modal decomposition is conducted to decouple all state variables. Besides, we denote the operating condition where the system is linearized as π_0. Finally, the decoupled representation of (1) is as follows

$$\dot{\boldsymbol{z}} = \Lambda \boldsymbol{z} + M^{-1}B\boldsymbol{u} \tag{2a}$$

$$\boldsymbol{y} = CM\boldsymbol{z} \tag{2b}$$

where $\boldsymbol{z} = \begin{bmatrix} z_1, z_2, \ldots, z_i, \ldots, z_n \end{bmatrix}^T$ and z_i is ith mode associating with eigenvalue λ_i; modal matrix $M = \begin{bmatrix} \boldsymbol{r}_1, \boldsymbol{r}_2, \ldots, \boldsymbol{r}_i, \ldots, \boldsymbol{r}_n \end{bmatrix}$, describing the mapping from vector $\boldsymbol{z}$ to state vector $\boldsymbol{x}$; $\Lambda = M^{-1}AM = \mathrm{diag}(\lambda_1, \lambda_2, \ldots, \lambda_n)$. M^{-1} can be denoted as $\begin{bmatrix} \boldsymbol{l}_1^T, \boldsymbol{l}_2^T, \ldots, \boldsymbol{l}_i^T, \ldots, \boldsymbol{l}_n^T \end{bmatrix}^T$, and $\boldsymbol{u}$ is $\begin{bmatrix} u_1, u_2, \cdots, u_q, \cdots, u_d \end{bmatrix}^T$.

Power systems are exposed to various kinds of small disturbances, e.g. load fluctuation, and sudden small change of generator voltage reference or mechanical power. In order to obtain a time-domain expression of the mode $\boldsymbol{z}$ under the above disturbances, each element in $\boldsymbol{u}$, say u_q, can be modeled as a step function as follows

$$u_q(t) = \begin{cases} u_q^0 & t \geq 0, \\ 0 & t < 0, \end{cases} \tag{3}$$

where u_q^0 is a stochastic value uniformly distributed within certain small range. At $t = 0$, $\boldsymbol{u}(0) = [u_1^0, u_2^0, \ldots u_q^0, \ldots u_d^0]^T$ and u_q^0 is uniformly distributed within a range of $[a, b]$, i.e.

$$u_q^0 \sim \mathcal{U}(a, b), \quad q \in \{1, 2, \cdots, d\}, \tag{4}$$

where $[a, b]$ is chosen such that the system can be represented by linearized model. Since all the elements in $\boldsymbol{u}$ are typically scaled to be in the per-unit form, in this paper, $[a, b]$ represents a range close to zero.

Under the above assumption, the kth potential measurement in $\boldsymbol{y}$ is expressed as

$$y_k = \sum_{i=1}^{n} \left[\boldsymbol{c}_k \boldsymbol{r}_i \left(\boldsymbol{l}_i \boldsymbol{x}_0 + \frac{\boldsymbol{l}_i B \boldsymbol{u}_0}{\lambda_i} \right) e^{\lambda_i t} \right] - \sum_{i=1}^{n} \left[\boldsymbol{c}_k \boldsymbol{r}_i \frac{\boldsymbol{l}_i B \boldsymbol{u}_0}{\lambda_i} \right] \tag{5}$$

where $\boldsymbol{c}_k$ is the kth row of C matrix. Equation (5) shows that one particular measurement can be represented as the summation of the exponential terms and the constant terms under a given disturbance, and its derivation is reported at Appendix A. Let $d_{ki} = \boldsymbol{c}_k \boldsymbol{r}_i (\boldsymbol{l}_i \boldsymbol{x}_0 + \boldsymbol{l}_i B \boldsymbol{u}_0 / \lambda_i)$. For the exponential terms associating with a pair of complex eigenvalues $\lambda_i = \alpha_i \pm j\beta_i$, their summation m_{ki} is

$$m_{ki} = d_{ki} e^{(\alpha_i + j\beta_i)t} + \bar{d}_{ki} e^{(\alpha_i - j\beta_i)t}$$
$$= 2 \left| \boldsymbol{c}_k \boldsymbol{r}_i \left(\boldsymbol{l}_i \boldsymbol{x}_0 + \frac{\boldsymbol{l}_i B \boldsymbol{u}_0}{\lambda_i} \right) \right| e^{\alpha_i t} \cos(\beta_i t + \phi_i) \tag{6}$$

where

$$\phi_i = \tan^{-1} \frac{\Im\left(\boldsymbol{c}_k \boldsymbol{r}_i \left(\boldsymbol{l}_i \boldsymbol{x}_0 + \sum_{q=1}^d \frac{\boldsymbol{l}_i \boldsymbol{b}_q u_q^0}{\lambda_i}\right)\right)}{\Re\left(\boldsymbol{c}_k \boldsymbol{r}_i \left(\boldsymbol{l}_i \boldsymbol{x}_0 + \sum_{q=1}^d \frac{\boldsymbol{l}_i \boldsymbol{b}_q u_q^0}{\lambda_i}\right)\right)}$$

and $\bar{(\cdot)}$ is the conjugate operator.

Now we define three concepts mentioned frequently in this paper. First, as we can see in (6), the summation of modes $z_i(t)$ and its conjugate $\bar{z}_i$ contributes to a sinusoidal term, which represents one of the frequency components in the oscillation waveform. In order to distinguish mode definition in (2), we define *complex mode* m_{ki} as the summation of modes associating with a pair of conjugate eigenvalues, i.e. λ_i and $\bar{\lambda}_i$. Second, the damping ratio $\xi_i = |\alpha_i|/\sqrt{\alpha_i^2 + \beta_i^2}$ and frequency β_i manifest themselves in (6), so we define that the complex mode $\hat{m}_{ki}$ is the *mode of interest* if the corresponding damping ratio $\hat{\xi}_i$ is less than the user-defined threshold ϵ, and frequency $\hat{\beta}_i$ falls into a certain range. Threshold ϵ typically ranges from 0.05 to 0.1, representing poorly-damped (complex) modes. It is worth noticing that we assume all modes of interest to be observable and controllable. Besides, various range of frequencies can be chosen for different purposes, e.g. it can be chosen to be from 0.628 rad/s to 6.28 rad/s (0.1 Hz to 1 Hz) for observing inter-area oscillations. Third, for the sake of convenience, we define

$$\psi_{ki} = 2 \left| \boldsymbol{c}_k \boldsymbol{r}_i \left(\boldsymbol{l}_i \boldsymbol{x}_0 + \frac{\boldsymbol{l}_i B \boldsymbol{u}_0}{\lambda_i}\right)\right| \tag{7}$$

as the *initial amplitude* of the complex mode i in the potential measurement k, representing the amplitude of the complex mode i at $t = 0$. Built upon the aforementioned definitions, (5) can be interpreted as a summation of complex modes, exponential terms with real eigenvalues and constant, which is

$$y_k(t) = \sum_{i \in \mathcal{M}} \psi_{ki} e^{\alpha_i t} \cos(\beta_i t + \phi_i)$$

$$+ \sum_{i \in \mathcal{N}} d_{ki} e^{\lambda_i t} - \sum_{i=1}^n \frac{\boldsymbol{c}_k \boldsymbol{r}_i \boldsymbol{l}_i B \boldsymbol{u}_0}{\lambda_i} \tag{8}$$

where

$$\mathcal{M} = \{i \in \mathbb{Z} \mid \Im \lambda_i > 0\}, \quad \mathcal{N} = \{i \in \mathbb{Z} \mid \Im \lambda_i = 0\} \tag{9}$$

Built upon the above notation, the set of indices of modes of interest $\hat{\mathcal{M}}$ can also be expressed as a subset of $\mathcal{M}$, which is

$$\hat{\mathcal{M}} = \left\{i \in \mathcal{M} \mid \frac{\Re(\lambda_i)}{|\lambda_i|} \le \epsilon, \quad \Im(\lambda_i) \in [\omega_l, \omega_h]\right\} \tag{10}$$

where values ϵ, ω_l and ω_h can be chosen as suggested above by users.

Equation (8) decomposes kth potential measurement from the theoretical perspective and connect meter-reading waveform $y_k(t)$ with complex modes. Although (8) indicates the potential measurement y_k incorporates components of all complex modes, not all modes can manifest themselves in y_k due to the eigen-structure of the system as well as the uncertainty of initial condition $\boldsymbol{x}_0$ and external disturbance $\boldsymbol{u}_0$. In fact, it is well accepted that each measurement has several dominant modes [2], [3]. Therefore, a potential measurement is said to be suitable

for observing a given complex mode if the complex mode can manifest itself as a dominant mode in that measurement.

The physical meaning of dominant modes can be illustrated in two ways. In the context of (8), a dominant complex mode intuitively means its initial amplitude should be relatively large compared to those of the other complex modes with similar damping ratio. From the perspective of frequency domain analysis, the height of the corresponding peak in the power spectral density (PSD) of the signal can be viewed as an equivalent indicator to suggest the dominant complex modes, since there should be a distinct peak right at the frequency of the complex mode if such frequency component contributes significantly to the total energy of the signal. Therefore, a potential measurement suitable for observing a complex mode m_i with frequency f_i should have a PSD with a distinct peak right at f_i, once m_i is excited. The above discussions suggest that the initial amplitude $\psi_{k,i}$ indicates the height of the corresponding peak in the PSD of measurement y_k and, therefore, serve as an indicator to select dominant modes in a given measurement and to construct the mapping from modes of interest to measurements.

However, the initial amplitude ψ_{ki} of a complex mode in a measurement is not sufficient for determining potential measurements suitable for oscillation monitoring, since it depends on uncertain disturbances and initial conditions, compromising the consistency of result of the dominant-mode selection. Hence, we need to introduce an index which is robust under various kinds of small disturbance in a statistical sense. Besides, such index should be able to describe the relative magnitude of the initial amplitude of each complex mode and determine dominant modes in a given measurement.

III. PROPOSED INDICATOR AND ALGORITHM FOR OBSERVING MODES OF INTEREST

In this section, modal participation ratio (MPR) is proposed for quantifying the significance of a certain mode in a potential measurement. Then, the comparison between the proposed MPR and several existing indices is presented, in order to demonstrate the advantage of the MPR. Finally, a two-layer algorithm is introduced for selecting existing PMUs and suggesting future PMU deployments to enhance the oscillation monitoring.

A. Modal Participation Ratio (MPR)

The MPR of the ith complex mode within the kth measurement is defined as follows:

$$p_{ki} = E\left(\frac{\psi_{ki}}{\sum_{v \in \mathcal{M}} \psi_{kv}}\right) = E\left(\frac{2\left|\boldsymbol{c}_k \boldsymbol{r}_i \left(\boldsymbol{l}_i \boldsymbol{x}_0 + \frac{\boldsymbol{l}_i B \boldsymbol{u}_0}{\lambda_i}\right)\right|}{\sum_{v \in \mathcal{M}}\left|\boldsymbol{c}_k \boldsymbol{r}_v \left(\boldsymbol{l}_v \boldsymbol{x}_0 + \frac{\boldsymbol{l}_v B \boldsymbol{u}_0}{\lambda_v}\right)\right|}\right) \tag{11}$$

where $E(\cdot)$ is expectation operator. Equation (11) is explained as follows. First, the fraction term describes the relative initial amplitude ψ_i of the complex mode i in a given measurement, compared with the rest of modes in y_k. Second, such relative initial amplitude is a stochastic variable as mentioned before, so an expectation operation is conducted in order to obtain an

average initial amplitude in the potential measurements based on the stochastic disturbance, rather than those due to a fixed disturbance. Third, a high value of p_{ki} suggests relatively high "proportion" of complex mode m_{ki} within given measurement y_k. If the complex mode m_{ki} happens to be of interest, the potential measurement y_k would be suitable for observing the poorly damped oscillations corresponding to m_{ki}, and distinct peak can be expected right at the frequency corresponding to m_{ki}. The MPR defined by (11) satisfies the two requirements presented at the end of Section II.

Recall x in (1) represents the state deviation from the steady state of the system, then x is a zero vector in the steady state. Besides, the disturbance is typically injected into the system through the input vector u rather than the direct perturbation of the internal state variables x. Then the initial condition is assumed to be a zero vector. Therefore, (11) reduces to

$$p_{ki} = E\left(\frac{2\left|c_k r_i l_i B u_0 \lambda_i^{-1}\right|}{\sum_{v\in\mathcal{M}}\left|c_k r_v l_v B u_0 \lambda_v^{-1}\right|}\right), \quad i\in\mathcal{M} \qquad (12)$$

which can be evaluated by Monte Carlo Simulation. It is worth pointing out that u_0 cannot cancel out in (12) since there are absolute operations in the denominator of (12). Meanwhile, (7) reduces to

$$\psi_{ki} = 2\left|c_k r_i l_i B u_0 \lambda_i^{-1}\right|, \quad i\in\mathcal{M} \qquad (13)$$

For the modes corresponding to real eigenvalues, its MPR and initial amplitude are forced to be zero, i.e.,

$$p_{ki} = \psi_{ki} = 0, \quad i\notin\mathcal{M} \qquad (14)$$

Built upon (12), (13) and (14), all MPRs and initial amplitudes can be organized into the matrix form, namely, the *MPR matrix* $P = [p_{ki}]$ and the *initial amplitude matrix* $\Psi = [\psi_{ki}]$, which serve as intermediate indicators for calculating MPR matrix in the sequel. In the matrix P and Ψ, the kth row corresponds to the kth potential measurement and the ith column corresponds to the ith complex mode. Besides, the algorithm for computing these two matrices runs as in Algorithm 1.

B. Comparison With Existing Concepts

The other two candidate indices relevant to our problem are the mode in output participation factor [12] and the geometric measure [9]. In this section, we conduct conceptual comparison between MPR and these two existing indices.

The modes in output participation factor is built upon mode in state participation factor introduced in [13] and is defined as follows

$$p_{ki} := E\left(\frac{l_i x_0 c_k r_i + \bar{l}_i x_0 c_k \bar{r}_i}{y_k(0)}\right), \qquad (15)$$

it measures the participation of ith complex mode in the kth potential measurement. In (15), disturbance uncertainties are considered to be from the initial state vector x_0. However, in this paper, we assume disturbance uncertainties come from the input vector u and each component in u is modeled as a step change with a stochastic amplitude. This assumption makes

---

Algorithm 1: Computing MPR matrix.

1: Specify Monte Carlo simulation times T_{mc}.
2: Calculate Λ, M, M^{-1} based on A matrix in (1).
3: Find set $\mathcal{M}$ based on (9).
4: $\Delta \leftarrow \mathbf{0}_{m,n}$ [2].
5: **for** $t_{\mathrm{mc}} = 1$ **to** T_{mc} **do**
6:     Generate a set of uniformly distributed random values showing as (4) and set it as u_0.
7:     Calculate each element ψ_{ki} in Ψ by (13) and (14).
8:     Obtain normalized version of matrix $\Psi = [\psi_{ki}]$ by

$$\psi_{ki} \leftarrow \frac{\psi_{ki}}{\sum_{v\in\mathcal{M}}\psi_{kv}}$$

9:     $\Delta \leftarrow \Delta + \Psi$;
10: **end for**
11: Obtain the MPR matrix by $P = T_{\mathrm{mc}}^{-1}\Delta$.

---

more physical sense, since it intuitively can represent abrupt changes of loads and generator setpoints at certain time instant, which may excite some critical modes. In order to scrutinize the physical meaning of mode in output participation factor (MOPF) and to make a fair comparison between MPR and MOPF, we *temporarily* assume disturbances directly impact the initial state vector x_0 and eliminate the output term Bu in (1). Then we find that the process of defining the MPR in (11) and the factor in (15) share similarity in terms of dealing with uncertainty in the system. Both concepts assumes that the evolution of complex modes does not only depend on the system inherent property, i.e., the eigen-structure, but are also determined by the disturbance uncertainties. Hence, both concepts consider the effect of disturbance uncertainties.

However, the physical meanings of these two factors are different. Under the temporary assumption on the source of disturbances, the complex mode m_{ki} in (6) reduces into

$$m_{ki} = 2\left|l_i x_0 c_k r_i\right| e^{\alpha_i t}\cos(\beta_i t + \phi_i) \qquad (16)$$

where

$$\phi_i = \tan^{-1}\frac{\Im(l_i x_0 c_k r_i)}{\Re(l_i x_0 c_k r_i)}.$$

At $t = 0$, $m_{ki}(0) = \Re(l_i x_0 c_k r_i)$, which exactly is numerator of (15). Therefore, the mode in output participation factor describes the percentage of the complex mode i in the initial value of kth output y_{k0}. If a potential measurement y_k can be viewed as the superposition of complex modes, decaying exponential terms and a constant as in (8), the mode in output participation factor in (15) can be employed to suggest the relative magnitudes of complex modes, rather than their initial amplitudes. However, the initial amplitude of the complex mode serves as a direct indicator of the height of the corresponding peak in the PSD, whereas the factor in (15) only characterizes the initial value of m_{ki} in (16), which is a lower bound of the initial amplitude. Therefore, there is no direct connection between the

---

[2] $\mathbf{0}_{m,n}$ is a zero matrix with m rows and n columns.

Algorithm 2: Layer 1: the existing signals selection.

1: $H \leftarrow \mathbf{0}_{m,n}$; find $\hat{\mathcal{M}}$ by (10); $\hat{\mathcal{M}}_{\text{observed}} \leftarrow \varnothing$.
2: **for** $i \in \hat{\mathcal{M}}$ **do**
3:   Find $\mathcal{K}_i$ by (18).
4:   $h_{vi} \leftarrow 1, \quad \forall v \in \mathcal{K}_i$.
5:   **for** $k \in \mathcal{B}$ **do**
6:     **if** $\mathcal{G}_k \cap \mathcal{K}_i \neq \varnothing$ **then**
7:       $\hat{\mathcal{M}}_{\text{observed}} \leftarrow \hat{\mathcal{M}}_{\text{observed}} \cup \{i\}$.
8:       Mode of interest i could be observed by the
         PMU installed at bus k via measurement
         $\arg \max\limits_{v \in \mathcal{G}_k \cap \mathcal{K}_i} p_{vi}$.
9:     **end if**
10:   **end for**
11: **end for**
12: **if** $\hat{\mathcal{M}} - \hat{\mathcal{M}}_{\text{observed}} = \varnothing$ **then**
13:   All modes of interest can be reliably captured by
       existing PMUs.
14: **else**
15:   Further deployment of PMU is needed.
16: **end if**

---

peaks in PSD and MOPF. This renders (15) improper to serve as an indicator for identifying critical PMU signals to monitor the oscillation modes of interest, even though disturbances are assumed to be from initial state vector $\boldsymbol{x}_0$. It is worth emphasizing that, when computing MPR, the disturbance uncertainty is considered to be from the input vector u and the impact of matrix B cannot be eliminated.

Geometric measure (GM) overcomes the limitation that Popov-Belevitch-Hautus (PBH) test only can offer a yes-or-no answer, and is designed to measure the modal controllability and observability [9]. The GM of modal observability of mode i for system (1) in measurement k is defined as follows [9]

$$g_{k,i} = \cos \left[\theta(\boldsymbol{c}_k, \boldsymbol{r}_i^T) \right] = \frac{|\boldsymbol{c}_k \boldsymbol{r}_i|}{||\boldsymbol{c}_k|| \, ||\boldsymbol{r}_i||} \quad (17)$$

where $|\cdot|$ is the magnitude of a complex value and $||\cdot||$ is 2-norm of a vector. Though its physical meaning can be explained from energy point of view [9], in the context of capturing modes of interest directly by decomposing raw measurements, such an explanation becomes obscured. Besides, all information needed for computing GM is from the inherent property of the system model, i.e., measurement vector $\boldsymbol{c}_k$ and right eigenvector $\boldsymbol{r}_i$, but no characteristics from uncertain disturbances are utilized. According to (13), the initial amplitude of complex mode i in measurement k depends both on structural parameters of power systems, i.e., $\boldsymbol{c}_k \boldsymbol{r}_i \boldsymbol{l}_i B$ and λ_i, and uncertain disturbances $\boldsymbol{u}_0$. Admittedly, the uncertain disturbance $\boldsymbol{u}_0$ does not play a role on the initial amplitude when $\boldsymbol{c}_k \boldsymbol{r}_i \boldsymbol{l}_i B = 0$. However, the product of $\boldsymbol{c}_k \boldsymbol{r}_i$ and $\boldsymbol{l}_i B$ may not be a "perfect" zero in most practical case, unless the complex mode i is either unobservable, i.e., $\boldsymbol{c}_k \boldsymbol{r}_i = 0$ or uncontrollable i.e., $\boldsymbol{l}_i B = 0$, which is out of the scope of this study. Further comparison will also be presented in part IV via simulation.

C. Threshold Selection for Dominant Complex Mode in Given Measurement

In this section, we present a quantitative threshold in terms of initial amplitude ψ_{ki} to determine the suitable signals for observing a given modes of interest. The k-th candidate signal is said to be suitable for observing the i-th complex mode if its MPR p_{ki} satisfies $p_{ki} \geq \gamma \sup_{v \in [1,2,\cdots,m]} p_{vi}$, where γ is a user-defined parameter and is empirically set to be 0.75 in this paper. Meanwhile, we define

$$\mathcal{K}_i = \left\{ i \in \mathbb{Z} \mid p_{ki} \geq \gamma \sup_{v \in \mathcal{M}} p_{kv}, \quad i \in \mathcal{M} \right\}. \quad (18)$$

$\mathcal{K}_i$ in (18) can be employed to find the indices of the possible measurements suitable for observing a given complex mode i.

D. Hierarchical Scheme for Optimal PMU Placement and Signal Selection

Some PMUs have already been deployed in the system based on either engineering intuition or requirements of standards, so the classical PMU-placement problem can be further broken into the following sub-problems: 1) identify the existing PMU signals that are most appropriate for observing a particular mode of interest; 2) identify the best locations for installing new PMUs, which could observe a particular mode that is unobservable using existing PMUs.

The first layer of the algorithm checks whether the further deployment of PMUs is needed and identify the best PMU signals for observing the modes of interest. Typically, one PMU has multiple channels, which allows us to observe all kinds of measurements relative to the bus where this PMU is installed. Suppose the set $\mathcal{B}$ collects the indices of the buses equipped with PMUs and each element in the set $\mathcal{G}_k$ represents the indice of PMU channel installed at Bus k, then the first-layer algorithm is presented as follows:

The set $\hat{\mathcal{M}}_{\text{observed}}$ stores the indices of complex modes which cannot be reliably observed from existing PMUs, so further deployment should be conducted for observing the complex modes in $\hat{\mathcal{M}}_{\text{observed}}$. In order to limit or minimize the number of further deployed PMUs, the selected buses for installing PMUs should allow us to observe as many modes of interest as possible using PMU signals from various channels.

For the sake of convenience, the following definitions are presented. Suppose the system represented by (1) has m' buses, each bus includes several potential measurements in $\boldsymbol{y}$. Besides, $m' \times n$ matrix $\hat{H} = [\hat{h}_{kv}]$ is denoted by $[\hat{\boldsymbol{h}}_1^T, \hat{\boldsymbol{h}}_2^T, \cdots, \hat{\boldsymbol{h}}_k^T, \cdots, \hat{\boldsymbol{h}}_{m'}^T]^T$ where $\hat{\boldsymbol{h}}_k \in \mathbb{R}^n$ is a row vector. Meanwhile, $\hat{H}$ can also be denoted by $[\hat{\boldsymbol{h}}'_1, \hat{\boldsymbol{h}}'_2, \cdots, \hat{\boldsymbol{h}}'_i, \cdots, \hat{\boldsymbol{h}}'_n]$, where $\hat{\boldsymbol{h}}'_i \in \mathbb{R}^{m'}$ is a column vector. Similarly, $m \times n$ matrix H can be denoted by $[\boldsymbol{h}_1^T, \boldsymbol{h}_2^T, \cdots, \boldsymbol{h}_v^T, \cdots, \boldsymbol{h}_{m'}^T]^T$.

Then the second layer algorithm is introduced to identify the optimal locations for installing new PMUs, in order to observe the modes of interest that are unobservable using existing PMUs.

Algorithm 3: Layer 2: further deployment of PMUs.

1: $\hat{H} \leftarrow \mathbf{0}_{n,m'}$.
2: **for** $k = 1$ **to** m' **do**
3:    $\hat{\boldsymbol{h}}_k \leftarrow \sum_{v \in \mathcal{G}_k} \boldsymbol{h}_v$.
4:    $\hat{h}_{kv} \leftarrow 1, \quad \forall v \in \{i \in \mathbb{Z} \mid h_{ki} > 1\}$.
5: **end for**
6: $\hat{\mathcal{M}}_n \leftarrow \hat{\mathcal{M}} - \hat{\mathcal{M}}_{\text{observed}}$.
7: **while** $\hat{\mathcal{M}}_n \neq \varnothing$ **do**
8:    $\boldsymbol{s} = \sum_{i \in \hat{\mathcal{M}}_n} \hat{\boldsymbol{h}}'_i$, denoting by
      $[s_1, s_2, \cdots, s_k, \cdots, s_{m'}]^T$
9:    PMU should be installed in $\hat{k}$-th bus, where
$$\hat{k} = \arg\max_k s_k.$$
10:    Find $\mathcal{I}_{\hat{k}}$ by $\mathcal{I}_{\hat{k}} = \{i \in \mathbb{Z} \mid \hat{h}_{\hat{k}i} = 1\}$.
11:    **for** $k \in \mathcal{G}_{\hat{k}}$ **do**
12:       Find $\mathcal{I}_k$ by $\mathcal{I}_k = \{i \in \mathbb{Z} \mid h_{ki} = 1\}$.
13:       **if** $\mathcal{I}_k \cap \mathcal{I}_{\hat{k}} \neq \varnothing$ **then**
14:          Mode of interest $\mathcal{I}_k \cap \mathcal{I}_{\hat{k}}$ could be observed by
          the PMU installed at bus $\hat{k}$ via measurement k.
15:       **end if**
16:    **end for**
17:    $\hat{\mathcal{M}}_n \leftarrow \hat{\mathcal{M}}_n - \mathcal{I}_{\hat{k}}$.
18: **end while**

It is worth pointing out that the proposed two-layer algorithm also works in systems without existing PMUs. In this case, layer 1 is skipped due to $\mathcal{B} = \varnothing$.

E. Online Scheme for Monitoring Critical Power System Oscillations Based on Two-layer Algorithm

In power systems, there are several qualitatively different operating conditions due to seasonal load levels and different network topologies [14]. What we propose could be potentially coupled with an online screen tool which determines which scenario the system conditions belong to. Suggested use case can be described by the following two-step approach:

1) Off-Line Study: Let the set $\Pi = \{\pi_1, \pi_2, \cdots, \pi_j, \cdots, \pi_w\}$ denote the collection of w operating scenarios identified during off-line studies. Each operating scenario represents a specific loading condition and topology of the system. For each operating scenario $\pi_j \in \Pi$, the power system can be linearized around the operating scenario π_j and the corresponding A, B and C matrix of the linearized system model can be obtained. Built upon these matrices, the proposed algorithm embedded with MPR can suggest location and/or selection of PMUs in order to most effectively observe modes of interest under the operating scenario π_j. Then, under the operating scenario π_j, we use $\mathcal{M}_{\pi_i}$ and $k_i^{\pi_j}$ to denote the set of complex modes of interest and the measurements suitable for monitoring complex mode i, respectively. Finally, the one-to-one mapping between modes of interest under various operating scenarios and the selected
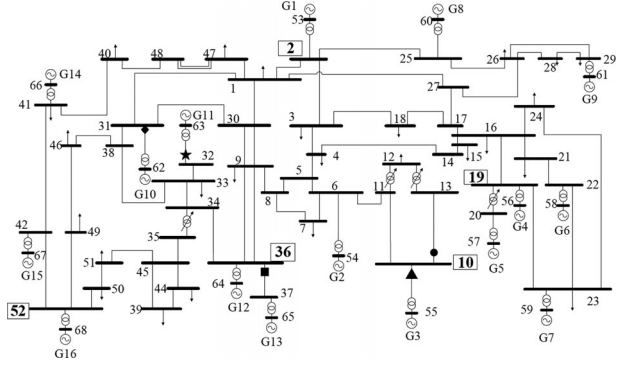

Fig. 1.   68-bus test system [16]: Numbers of buses equipping with PMU are boxed; the geographic locations of each selected channel in Table I are marked.

signals can form a lookup table, which can be utilized in the real-time monitoring of critical power system oscillations.

2) Online Application: During real-time operation of power systems, the Energy Management System (EMS) will report the current operating scenario π_j. π_j reflects the current loading condition and topology of the system. Based on π_j, the PMU signals suitable for monitoring modes of interest, i.e., $k_i^{\pi_j}$ for all $i \in \mathcal{M}_{\pi_j}$, can be found in the lookup table created during off-line study, and they will be displayed in front of system operators. Once a poorly-damped mode is excited, system operators will be informed by a distinct peak around the frequency of the mode in the PSD of the selected signal. For example, suppose there is a fault that causes the topology of a power system to change, we use $\pi_{j'}$ to denote the operating scenario after the topology change. Several modes collected by set $\mathcal{M}_{\pi_{j'}}$ might be of interest to system operators and each mode can be effectively monitored by the corresponding measurement selected by the lookup table.

Admittedly, exhausting the representative scenarios Π that can explain every possible operating conditions may require significant efforts for large-scale power systems. During the initial stage of the proposed scheme, however, one can only include the scenarios corresponding to severe operating conditions, e.g., operating conditions when the system is heavily loaded, into set Π. As the study on the power systems becomes more and more thorough, it is promising to enumerate the representative scenarios that can explain most possible operating conditions.

IV. CASE STUDIES

The performance of newly-introduced indicator MPR and the two-layer algorithm is validated in the modified benchmark 68-bus system (Fig. 1) and the Northeastern Power Council (NPCC) 140-bus system. The raw parameters for both systems are available in the Power System Toolbox (PST) [15]. In the both cases, the threshold ϵ, f_l and f_h in (10) are set to be 5%, 0.1 Hz and 2 Hz, respectively. Besides, stochastic disturbances in both test systems are modeled as random changes on voltage references of voltage regulators $\boldsymbol{V}_{ref}$, mechanical power injections $\boldsymbol{P}_m$ and real and reactive power of loads $\boldsymbol{P}_l$ and $\boldsymbol{Q}_l$. The above three components constitutes the vector $\boldsymbol{u}_0$ and each element u_q^0 is uniformly distributed within $[-0.1, 0.1]$.

TABLE I
RESULT OF TWO-LAYER ALGORITHM FOR 68-BUS SYSTEM

Layer	Selected Channel	i	$\xi_i(\%)$	$f_i(Hz)$
1	P from Bus 10 to 13	181	4.96	1.11
	P from Bus 36 to 37	183	3.62	1.16
	P from Bus 10 to 55	189	3.98	1.27
2	P from Bus 31 to 62	193	3.06	1.30
	P from Bus 32 to 63	207	3.64	1.88

A. Results of Two-Layer Algorithm and Its Validation for the 68-bus System

1) 68-Bus System Description: For the 68-bus system, three main modifications are made to the raw parameters. First, in order to obtain poorly-damped complex modes, the gain-washout time constant of the power system stabilizers (PSS) at generator 9 is set to 200, and the PSSs at the rest of generators are disabled. Second, load modulations of real and reactive power are added to simulate the stochastic load fluctuation. Third, the load and generation levels are set to be 65% of the original level. Then, all the modal parameters of modes of interest listed in Table I can be calculated based on matrix A, B and C in (1).

In this test case, several existing PMUs are introduced, based on the following engineering intuition: First, generators with relatively large capacity are considered as "important" generators, thus buses near those generators should be equipped with PMUs. Second, PMU deployment should spread over the whole grid, rather than focus on a limited area. Hence, the existing PMUs are installed at Bus 2, 10, 19, 36 and 52.

2) Results for the Two-Layer Algorithm: Table I contains the result of each layer of the algorithm. The first-layer algorithm selects PMU channels specifically for observing complex mode 183 and 189 from existing PMUs. Since not all the modes of interest can be observed from existing PMUs, further deployment is needed. Then the second-layer algorithm identifies the suitable locations for installing new PMUs. Finally, we expect that modes of interest should manifest themselves in waveforms recorded by their corresponding channels, if those complex modes are excited.

3) PSD Validation: In order to compare the performance between selected and unselected PMUs in terms of observing modes of interest, waveforms recorded by all the potential measurements under a stochastic disturbance should be obtained. To achieve this, the test system is represented by the state-space model in (1) with 98×1 input vector $\boldsymbol{u}(t)$ and 525×1 output vector $\boldsymbol{y}(t)$. After a 30-second simulation, the output vector $\boldsymbol{y}$ offers 525 sets of time series and each of them contains 30×60 samples, representing 60-second waveforms recorded by 525 measurement channels of PMUs with a sampling rate of 60 Hz. Besides, Gaussian noise with a signal-to-noise ratio (SNR) of 45 dB is added to each set of time series. Finally, frequency components of each waveform can be analyzed via Fast Fourier Transformation (FFT).

In our test case, instead of monitoring all the 525 waveforms, we only need to monitor five PMU channels for determining whether the modes of interest are excited. If a mode of interest
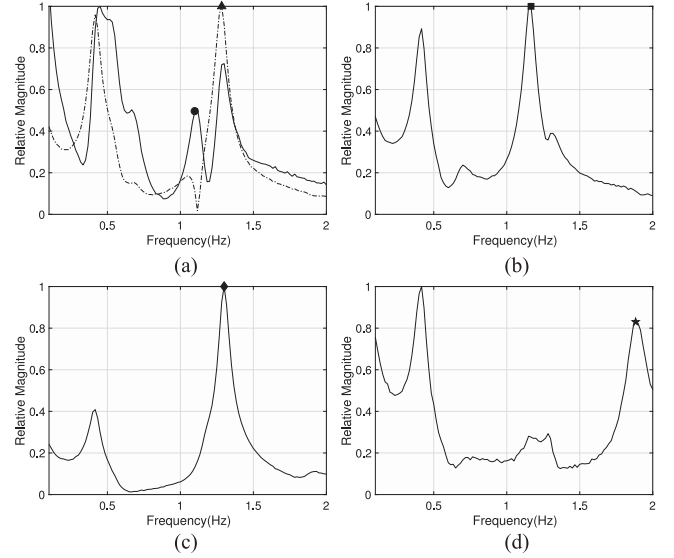

Fig. 2. PSD of selected signals for 68-bus system in Table I. The marked peaks indicate all 5 modes of interest are excited: (a) Bus 10 to 13 P (solid line), Bus 10 to 55 (dot line), ● mode 181 at 1.11Hz, ▲ mode 189 at 1.27Hz; (b) Bus 36 to 37 P, ■ mode 183 at 1.16 Hz; (c) Bus 31 to 62 ♦ mode 193 at 1.3Hz; (d) Bus 32 to 63, ★ mode 207 at 1.88Hz.

TABLE II
RESULT OF TWO-LAYER ALGORITHM FOR THE NPCC 140-BUS SYSTEM

Bus	Selected Channel	i	$\xi_i(\%)$	f_i (Hz)
71	Frequency Deviation	295	4.53	0.91
8	P from Bus 8 to 9	181	1.37	0.62
	P from Bus 8 to 18	293	3.79	0.89
53	P from Bus 53 to 52	325	4.51	1.16
	P from Bus 53 to 65	371	2.53	1.64
68	Frequency deviation	375	2.41	1.68
		385	2.05	1.99
92	P from Bus 92 to 97	327	4.82	1.22
	Q from Bus 92 to 97	359	3.15	1.42
117	P from Bus 117 to 121	321	4.51	1.16
	P from Bus 117 to 119	383	2.15	1.85
118	P from Bus 118 to 123	365	2.98	1.49
		373	2.41	1.68

is excited by a disturbance, this complex mode would manifest itself as a dominant complex mode in the selected PMU channel specifically selected for it. Therefore, a peak would appear right at its frequency in the PSD. Fig. 2 presents the PSD of waveforms recorded by selected channels under certain disturbance. These figures inform operators that all the five modes of interest are excited, due to the five peaks at frequencies of these complex modes.

B. Results of Two-Layer Algorithm and Its Validation for the NPCC 140-bus System

For the NPCC 140-bus system, load modulations of real and reactive power are added to the original system provided by PST. Then, the matrix A, B and C in (1) can be extracted by PST, and all the modes of interest in this case are listed in Table II. Besides, based on the engineering intuition, the existing PMUs are installed at Bus 22, 54, 71, 101 and 135. Table II presents
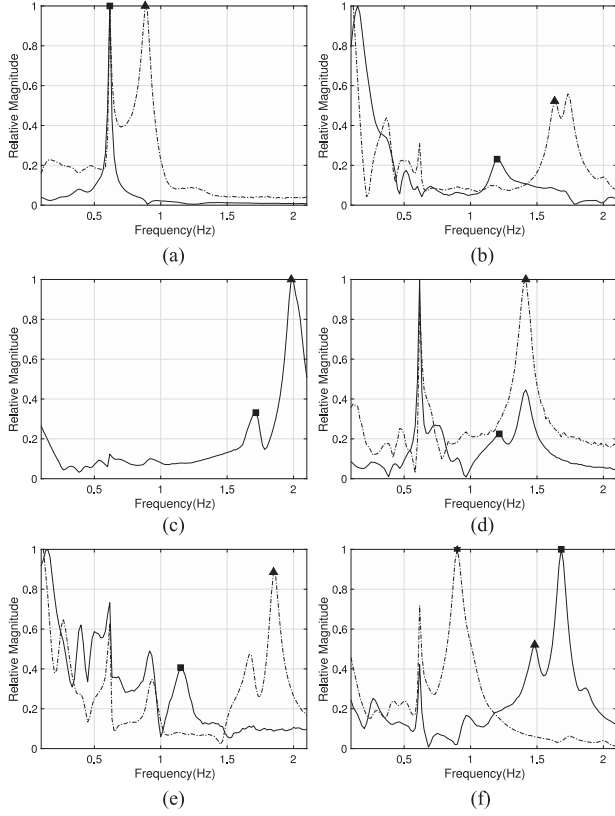
Fig. 3. PSD of selected signals for NPCC 140-bus system in Table II.(a) Bus 8 to 9 (solid line), 0.62Hz (square); Bus 8 to 18 P (dot line), 0.89Hz (triangle); (b) Bus 53 to 52 (solid line), 1.16Hz (square); Bus 53 to 65 P (dot line), 1.64Hz (triangle); (c) Bus 68 Freq (solid line), 1.68Hz (square), 1.99Hz (triangle); (d) Bus 92 to 97 P (solid line), 1.22Hz (square), Bus 92 to 97 Q (dot line), 1.42Hz (triangle); (e) Bus 117 to 121 P (solid line), 1.16Hz (square), Bus 117 to 119 P (dot line), 1.85Hz (triangle); (f) Bus 118 to 123 P (solid line), 1.49Hz (square), 1.68Hz (triangle); Bus 71 freq (dot line), 0.19Hz (hexagram).

the result of each layer of algorithm. The existing PMU at Bus 71 is selected for observing the complex mode 295, and the locations of PMUs for observing the rest of modes of interest are also suggested by the second layer algorithm. As we can observe from Table II, in terms of bus selection, the second layer algorithm gives high priorities to the buses enabling us to observe multiple modes of interest. Hence, suppose there is no existing PMU, only 7 buses should be equipped with PMUs, although there are 13 modes of interest. Besides, Fig. 3 shows each modes of interest manifests itself in the signal selected for monitoring it.

C. Convergence Test of MPR

The MPR is calculated via Monte Carlo simulation, so a natural question is whether the result of MPR depends on the simulation time T_{mc}. Fig. 4 visualizes the variation of 5 elements in MPR as simulation times T_{mc} changes from 50 to 10,000 times ($p_{262,183}$: solid line, $p_{201,189}$: dash-dot line, $p_{195,181}$: dash line, $p_{260,193}$: dot line and $p_{261,207}$: dash-circle line). As shown in Fig. 4, the selected elements in the MPR matrix tend to be bounded as simulation time T_{mc} increases.
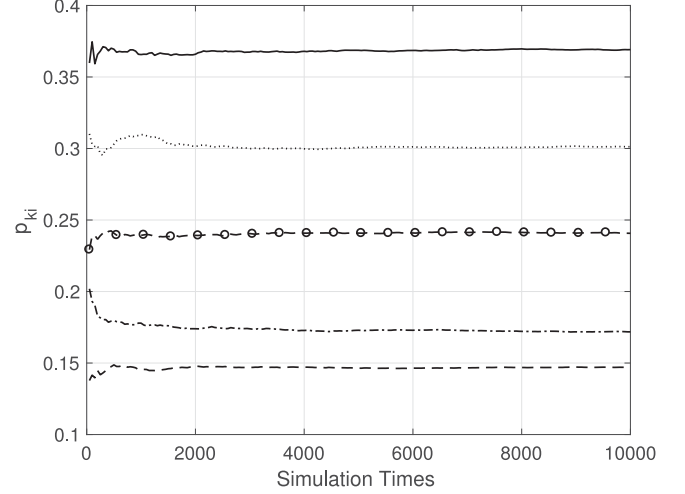

Fig. 4. Convergence test for 5 selected elements in MPR matrix.
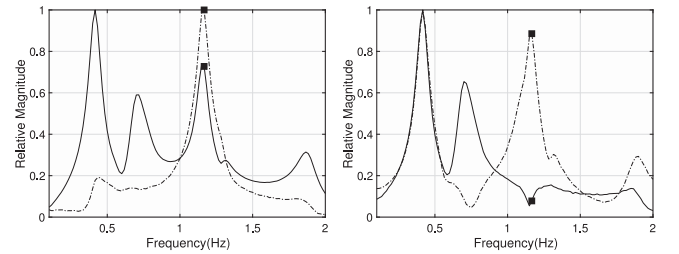

Fig. 5. Impact of uncertain disturbance on the PSD of signals.

D. Impact of Uncertain Disturbance on Proportion of Complex Modes in Measurements

Under certain disturbance, some unselected signals seem to be suitable for observing modes of interest. In Fig. 5, the left figure represents the PSD of the selected signal, i.e. the real power waveform from Bus 36 to Bus 37; the right figure represents the PSD of the unselected signal, i.e. the real power from Bus 65 to Bus 37. Under disturbance $\boldsymbol{u}_1$, the dash line at the right figure shows a distinct peak right at the frequency of the mode of interest, then the unselected signal might be also considered suitable for observing complex mode 183. However, under another disturbance $\boldsymbol{u}_2$, a distinct peak corresponding to complex mode 183 is presented in the selected signals (solid line in right figure), whereas no distinct peak corresponding to the complex mode 183 can be observed from the unselected signals (solid line in left figure). Thus, the unselected signal might not be suitable for observing the complex mode 183. Although the disturbance uncertainties cause the variation in the of the peak marked with square, it is sufficient to conclude that complex mode 183 is excited based on the selected signal.

Another demonstrative scenario can be synthesized from right figure of Fig. 5 to articulate the necessity for this research. Suppose only the channel measuring real power from bus 65 to 37 is monitored, the operators may only observe the two uninterested complex modes below 1Hz, and might not be sure whether the complex mode 183 is excited when disturbance $\boldsymbol{u}_2$ happens. Therefore, they might not take any action due to
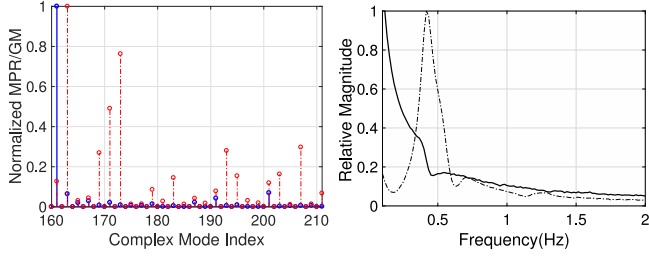
Fig. 6.   Performance Comparison between MPR and GM.

relatively high damping ratio of those two modes. However, the system is suffering from the sustained oscillation caused by complex mode 183, which may not be observed through the monitored PMU channel. However, if the PMU channel from bus 36 to bus 37 is monitored, the poorly-damped complex mode 183 could be observed by system operators.

E. Comparison With Geometric Measure

Now we present the performance comparison between MPR and GM in terms of observing complex modes. To perform comparison, the MPR $\hat{p}_{k,i}$ and GM $\hat{g}_{k,i}$ are normalized by dividing $\sup\limits_{v\in\mathcal{M}} p_{k,v}$ and $\sup\limits_{v\in\mathcal{M}} g_{k,v}$, respectively.

The channel measuring reactive power from bus 1 to 2 is selected for comparing the accuracy of the two indices. The left figure in Fig. 6 is the visualization of MPR (solid line) and GM (dash-dot line) for this channel. It shows an obvious discrepancy between MPR and GM: GM suggests this meter is suitable for observing the complex mode 163 with a frequency of 0.4162 Hz, whereas MPR indicates opposite results. If GM is reliable, we would expect a peak around 0.4162 Hz in PSD of the waveform recorded by this channel, when this complex mode is excited. However, according to the solid line in the right figure, complex the mode 163 does not manifest itself at the aforementioned channel, while it is indeed excited due to the appearance of a peak around 0.4162 Hz in the PSD of another PMU waveform (dash-dot line). Therefore, the proposed MPR method offers some advantage in terms of reliably identifying suitable PMU signals for modes of interest.

F. Robustness Test

In the preceding discussion, a set of measurements $\mathcal{K}_i$ suitable for observing the complex mode i is selected based on one loading condition and an exact system model in (18). However, one might expect to know the changes of the set $\mathcal{K}_i$ under other loading conditions, and whether the selected measurement set $\mathcal{K}_i$ can tolerate model errors. In this section, we explore the robustness of the proposed algorithm with respect to different levels of loading conditions and model errors.

1) Impact of Different Loading Conditions: For a given mode of interest i, we can use $\mathcal{K}_i^{\mathcal{C}_{\text{load}}}$ to represent the measurement set selected by (18) under one loading condition $\mathcal{C}_{\text{load}}$, i.e., $\mathcal{C}_{\text{load}} = \{100\%\}$. Meanwhile, one might wonder the changes of the result of the two-layer algorithm, $\mathcal{K}_i^{\bar{c}_{\text{load}}}$, under other loading conditions $\bar{c}_{\text{load}}$, compared with $\mathcal{K}_i^{\mathcal{C}_{\text{load}}}$. In order
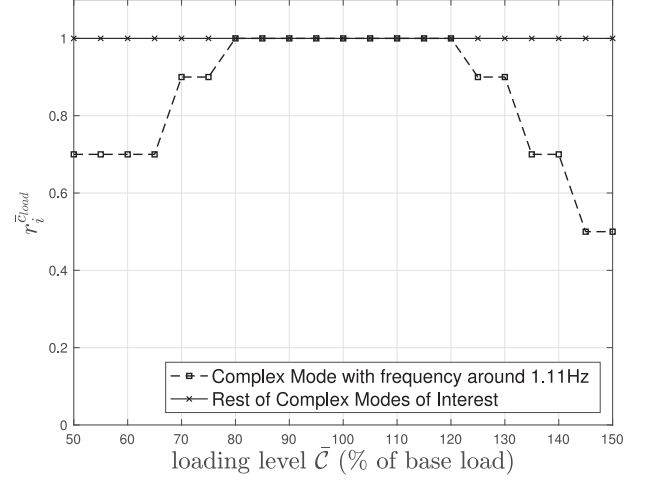

Fig. 7.   Visualization of $r_i^{\bar{c}_{\text{load}}}$ for the 68-bus system.

TABLE III
FREQUENCIES OF POORLY-DAMPED MODES WITH DIFFERENT
LEVELS OF MODEL ERROR

freq (Hz) $\diagdown$ c_{error} i	0%	5%	10%	15%	20%
181	1.1078	1.1114	1.1026	1.1107	1.0720
183	1.1577	1.1537	1.1775	1.2079	1.1965
189	1.2740	1.2871	1.2584	1.2471	1.2550
193	1.2779	1.2938	1.2674	1.2576	1.2607
207	1.8809	1.8921	1.9082	1.8201	1.9729

to quantify the overlap of results under two different loading condition, define $r_i^{\bar{c}_{\text{load}}}$ as $\left|\mathcal{K}_i^{\mathcal{C}_{\text{load}}} \cap \mathcal{K}_i^{\bar{c}_{\text{load}}}\right| / \left|\mathcal{K}_i^{\mathcal{C}_{\text{load}}}\right|$, **where $\bar{c}_{\text{load}} \in \{50\%, 55\%, \cdots, 150\%\}$ and each element represents the percentage of the loading condition in the original test case. Then $r_i^{\bar{c}_{\text{load}}}$ can be visualized as in Fig. 7. It suggests that the result of the first-layer algorithm under the loading condition $\mathcal{C}_{\text{load}}$ can also be applied in the system under the rest of the loading condition $\bar{c}_{\text{load}}$, for the complex modes with frequencies around 1.16 Hz, 1.27 Hz, 1.3 Hz and 1.88 Hz.

2) Impact of Different Levels of Model Errors: Similarly, we use $\mathcal{K}_i^0$ to denote the selected sets of measurements suitable for observing complex mode i, based on the "perfect" model. Then the parameters of all transmission lines and generators are modified by adding/reducing random percentages of their original values. The percentage is uniformly distributed within $[-c_{\text{error}}, c_{\text{error}}]$, where $c_{\text{error}} \in \{5\%, 10\%, 15\%, 20\%\}$. For the sake of convenience, we define c_{error} as the *level of model error*. Finally, $r_i^{c_{\text{error}}} = \mathcal{K}_i^0 \cap \mathcal{K}_i^{c_{\text{error}}} / \mathcal{K}_i^0$ characterizes the change of results due to model errors. Table IV indicates that the proposed algorithm can tolerate moderate model errors, e.g., no more than 5% of parameter changes.

Although the measurements suitable for monitoring modes of interest are selected based on an exact model in the preceding section, the proposed algorithm embedded with MPR allows some reasonable model errors. For example, suppose the level of model error is 5%, there are also 5 modes of interest with inaccurate modal frequencies as shown in the third column of Table III. Then the measurements suitable for observing each

TABLE IV
$r_i^{C_{\text{ERROR}}}$ OVER DIFFERENT LEVEL OF PARAMETER
ERRORS IN THE 68 BUS SYSTEM

$r_i^{C_{\text{error}}}$ $\diagdown$ C_{error} i	5%	10%	15%	20%
181	100%	76.92%	×[1]	×
183	100%	100%	100%	66.67%
189	100%	100%	66.67%	54.56%
193	100%	100%	50%	33.33%
207	100%	100%	×	70%

inaccurate modes are selected based on inaccurate model. According to Table IV, the result is the same with the case when the exact model is used, even though the measurements are selected based on an inaccurate model.

It is also possible that the actual critical modes are not in the vicinity of the modes calculated from offline models. In this case, system operators or planners should correct their first-principle model such that all mode of interest are properly included. Given active and ongoing model validation projects in power industry, as well as higher requirements of mandatory standards on model accuracy, it is not impossible to approximately characterize the actual critical modes from offline models in the near future.[3]

V. CONCLUSION

This paper introduced a robust indicator, MPR, for identifying critical PMU locations and signal channels, in order to better monitor power system oscillations with specific oscillation modes. Based on the proposed MPR, two-layer algorithm is presented. System operators and planners can benefit from this algorithm in the following two ways: 1) it identifies existing PMU devices and signal channels, which provides sufficient observability for critical oscillation modes; 2) it suggests optimal locations for further PMU deployments, in order to enhance the observability for critical oscillation modes. From a research perspective, this paper points out that the distribution of modal information among all measurements depends both on the system parameters and the characteristics of the disturbance.

APPENDIX A
DERIVATION OF TIME-DOMAIN SOLUTION OF MEASUREMENTS

Here, we present the derivation process for (5). Equation (2a) can be expanded as

$$\begin{bmatrix} \dot{z}_1 \\ \dot{z}_2 \\ \vdots \\ \dot{z}_i \\ \vdots \\ \dot{z}_n \end{bmatrix} = \begin{bmatrix} \lambda_1 & & & & & \\ & \lambda_2 & & & & \\ & & \ddots & & & \\ & & & \lambda_i & & \\ & & & & \ddots & \\ & & & & & \lambda_n \end{bmatrix} \begin{bmatrix} z_1 \\ z_2 \\ \vdots \\ z_i \\ \vdots \\ z_n \end{bmatrix}$$

$$+ \begin{bmatrix} \boldsymbol{l}_1\boldsymbol{b}_1 & \boldsymbol{l}_1\boldsymbol{b}_2 & \cdots & \boldsymbol{l}_1\boldsymbol{b}_q & \cdots & \boldsymbol{l}_1\boldsymbol{b}_d \\ \boldsymbol{l}_2\boldsymbol{b}_1 & \boldsymbol{l}_2\boldsymbol{b}_2 & \cdots & \boldsymbol{l}_2\boldsymbol{b}_q & \cdots & \boldsymbol{l}_2\boldsymbol{b}_d \\ \vdots & \vdots & \ddots & \vdots & \ddots & \vdots \\ \boldsymbol{l}_i\boldsymbol{b}_1 & \boldsymbol{l}_i\boldsymbol{b}_2 & \cdots & \boldsymbol{l}_i\boldsymbol{b}_q & \cdots & \boldsymbol{l}_i\boldsymbol{b}_d \\ \vdots & \vdots & \ddots & \vdots & \ddots & \vdots \\ \boldsymbol{l}_n\boldsymbol{b}_1 & \boldsymbol{l}_n\boldsymbol{b}_2 & \cdots & \boldsymbol{l}_n\boldsymbol{b}_q & \cdots & \boldsymbol{l}_n\boldsymbol{b}_d \end{bmatrix} \begin{bmatrix} u_1 \\ u_2 \\ \vdots \\ u_q \\ \vdots \\ u_d \end{bmatrix} \quad (19)$$

where $\boldsymbol{b}_q$ is the q-th column of B matrix in (1), and the rest notations are consistent with that in Section II. For i-th mode

$$\dot{z}_i = \lambda_i z_i + \boldsymbol{l}_i\boldsymbol{b}_1 u_1 + \boldsymbol{l}_i\boldsymbol{b}_2 u_2 + \cdots + \boldsymbol{l}_i\boldsymbol{b}_q u_q + \cdots + \boldsymbol{l}_i\boldsymbol{b}_d u_d \tag{20}$$

Then we conduct Laplace transform for both sides of (20) and obtain

$$z_i(s) = \frac{z_i^0}{(s - \lambda_i)} + \frac{1}{s - \lambda_i} \sum_{q=1}^{d} \frac{\boldsymbol{l}_i\boldsymbol{b}_q u_q^0}{\lambda_i} - \frac{1}{s} \sum_{q=1}^{d} \frac{\boldsymbol{l}_i\boldsymbol{b}_q u_q^0}{\lambda_i} \tag{21}$$

where z_i^0 is the value of i-th mode at $t = 0$ and u_q^0 has the same meaning as it in (3). Through inverse Laplace transform, the time-domain evolution of i-th mode can be obtained as follows:

$$z_i(t) = z_i^0 e^{\lambda_i t} + e^{\lambda_i t} \sum_{q=1}^{d} \frac{\boldsymbol{l}_i\boldsymbol{b}_q u_q^0}{\lambda_i} - \sum_{q=1}^{d} \frac{\boldsymbol{l}_i\boldsymbol{b}_q u_q^0}{\lambda_i} \tag{22}$$

Similarly, we expand (2b) as

$$\begin{bmatrix} y_1 \\ y_2 \\ \vdots \\ y_k \\ \vdots \\ y_m \end{bmatrix} = \begin{bmatrix} \boldsymbol{c}_1\boldsymbol{r}_1 & \boldsymbol{c}_1\boldsymbol{r}_2 & \cdots & \boldsymbol{c}_1\boldsymbol{r}_n \\ \boldsymbol{c}_2\boldsymbol{r}_1 & \boldsymbol{c}_2\boldsymbol{r}_2 & \cdots & \boldsymbol{c}_2\boldsymbol{r}_n \\ \vdots & \vdots & \ddots & \vdots \\ \boldsymbol{c}_k\boldsymbol{r}_1 & \boldsymbol{c}_k\boldsymbol{r}_2 & \cdots & \boldsymbol{c}_k\boldsymbol{r}_n \\ \vdots & \vdots & \ddots & \vdots \\ \boldsymbol{c}_m\boldsymbol{r}_1 & \boldsymbol{c}_m\boldsymbol{r}_2 & \cdots & \boldsymbol{c}_m\boldsymbol{r}_n \end{bmatrix} \begin{bmatrix} z_1 \\ z_2 \\ \vdots \\ z_i \\ \vdots \\ z_n \end{bmatrix} \tag{23}$$

Then the evolution of k-th measurement is

$$y_k = \sum_{i=1}^{n} \boldsymbol{c}_k\boldsymbol{r}_i \left(z_i^0 e^{\lambda_i t} + e^{\lambda_i t} \sum_{q=1}^{d} \frac{\boldsymbol{l}_i\boldsymbol{b}_q u_q^0}{\lambda_i} - \sum_{q=1}^{d} \frac{\boldsymbol{l}_i\boldsymbol{b}_q u_q^0}{\lambda_i} \right)$$

$$= \sum_{i=1}^{n} \left[\boldsymbol{c}_k\boldsymbol{r}_i \left(z_i^0 + \frac{\boldsymbol{l}_i B \boldsymbol{u}_0}{\lambda_i} \right) e^{\lambda_i t} \right] - \sum_{i=1}^{n} \left[\boldsymbol{c}_k\boldsymbol{r}_i \frac{\boldsymbol{l}_i B \boldsymbol{u}_0}{\lambda_i} \right] \tag{24}$$

Besides, the decoupled modes $\boldsymbol{z}$ are transformed from the original state variables $\boldsymbol{x}$ based on the relationship $\boldsymbol{z} = M^{-1}\boldsymbol{x}$. In particular, the i-th mode z_i at $t = 0$ can be obtained by

$$z_i^0 = \boldsymbol{l}_i \boldsymbol{x}_0 \tag{25}$$

Finally, plugging (25) into (24), we obtain (5).

REFERENCES

[1] L. Xie, Y. Chen, and P. R. Kumar, "Dimensionality reduction of synchrophasor data for early event detection: Linearized analysis," *IEEE Trans. Power Syst.*, vol. 29, no. 6, pp. 2784–2794, Nov. 2014.

[2] J. Ning, S. A. N. Sarmadi, and V. Venkatasubramanian, "Two-level ambient oscillation modal estimation from synchrophasor measurements," *IEEE Trans. Power Syst.*, vol. 30, no. 6, pp. 2913–2922, Nov. 2015.

[3] "×" indicates that the corresponding complex mode is not the one of interest.

[3] D. J. Trudnowski, J. W. Pierre, N. Zhou, J. F. Hauer, and M. Parashar, "Performance of three mode-meter block-processing algorithms for automated dynamic stability assessment," *IEEE Trans. Power Syst.*, vol. 23, no. 2, pp. 680–690, May 2008.

[4] J. W. Pierre, D. J. Trudnowski, and M. K. Donnelly, "Initial results in electromechanical mode identification from ambient data," *IEEE Trans. Power Syst.*, vol. 12, no. 3, pp. 1245–1251, Aug. 1997.

[5] R. W. Wies, J. W. Pierre, and D. J. Trudnowski, "Use of arma block processing for estimating stationary low-frequency electromechanical modes of power systems," *IEEE Trans. Power Syst.*, vol. 18, no. 1, pp. 167–173, Feb. 2003.

[6] J. Zhang, C. Wu, and Y. Han, "A power spectrum density based signal selection approach for electromechanical mode estimation," in *Proc. 2012 IEEE Power Energy Soc. Gen. Meet.*, Jul. 2012, pp. 1–7.

[7] V. S. Perić, X. Bombois, and L. Vanfretti, "Optimal signal selection for power system ambient mode estimation using a prediction error criterion," *IEEE Trans. Power Syst.*, vol. 31, no. 4, pp. 2621–2633, Jul. 2016.

[8] I. J. Perez-arriaga, G. C. Verghese, and F. C. Schweppe, "Selective modal analysis with applications to electric power systems, part i: Heuristic introduction," *IEEE Trans. Power App. Syst.*, vol. PAS-101, no. 9, pp. 3117–3125, Sep. 1982.

[9] A. Hamdan and A. Elabdalla, "Geometric measures of modal controllability and observability of power system models," *Electr. Power Syst. Res.*, vol. 15, no. 2, pp. 147–155, 1988.

[10] A. M. Almutairi and J. V. Milanovic, "Comparison of different methods for optimal placement of PMUS," in *Proc. 2009 IEEE Bucharest PowerTech*, Jun. 2009, pp. 1–6.

[11] A. Heniche and I. Karnwa, "Control loops selection to damp inter-area oscillations of electrical networks," *IEEE Trans. Power Syst.*, vol. 17, no. 2, pp. 378–384, May 2002.

[12] L. Sheng, E. H. Abed, M. A. Hassouneh, H. Yang, and M. S. Saad, "Mode in output participation factors for linear systems," in *Proc. 2010 Amer. Control Conf.*, Jun. 2010, pp. 956–961.

[13] W. A. Hashlamoun, M. A. Hassouneh, and E. H. Abed, "New results on modal participation factors: Revealing a previously unknown dichotomy," *IEEE Trans. Autom. Control*, vol. 54, no. 7, pp. 1439–1449, Jul. 2009.

[14] I. Kamwa and R. Grondin, "PMU configuration for system dynamic performance measurement in large, multiarea power systems," *IEEE Trans. Power Syst.*, vol. 17, no. 2, pp. 385–394, May 2002.

[15] J. H. Chow and K. W. Cheung, "A toolbox for power system dynamics and control engineering education and research," *IEEE Trans. Power Syst.*, vol. 7, no. 4, pp. 1559–1564, Nov. 1992.

[16] H. Bevrani, M. Watanabe, and Y. Mitani, *Power System Monitoring and Control*. Hoboken, NJ, USA: Wiley, 2014.
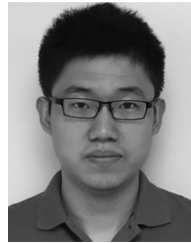
Tong Huang (S'16) received the B.E. degree in electric power engineering and its automation from North China Electric Power University, Baoding, China, in 2013 and the M.S. degree in electrical engineering from Texas A&M University, College Station, TX, USA, in 2017, where he is currently working toward the Ph.D. degree. His research interests include power system stability, security, and wide-area monitoring and control systems.
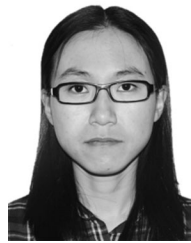
Meng Wu (S'14) received the B.E. degree from Tianjin University, Tianjin, China, in 2010, and the M.Eng. degree from Cornell University, Ithaca, NY, USA, in 2011, both in electrical engineering. She is currently working toward the Ph.D. degree at Texas A&M University, College Station, TX, USA. From 2011 to 2012, she was an R&D Engineer at China Electric Power Research Institute, Beijing, China and Beijing Sifang Automation Co. Ltd., Beijing, China from 2012 to 2013. Her research interests include power system modeling, stability analysis, renewable energy integration, and wide-area monitoring and control systems.
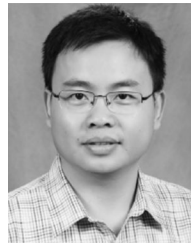
Le Xie (S'05–M'10–SM'16) received the B.E. degree in electrical engineering from Tsinghua University, Beijing, China, in 2004, the M.S. degree in engineering sciences from Harvard University, Cambridge, MA, USA, in 2005, and the Ph.D. degree from the Department of Electrical and Computer Engineering, Carnegie Mellon University, Pittsburgh, PA, USA, in 2009. He is currently an Associate Professor with the Department of Electrical and Computer Engineering, Texas A&M University, College Station, TX, USA.

His research interests include modeling and control of large-scale complex systems, smart grids application with renewable energy resources, and electricity markets.